Int. J. Electrochem. Sci., 8 **(2013)** 3939 - 3952

International Journal of ELECTROCHEMICAL SCIENCE
www.electrochemsci.org

Analysis by CFD Tool to Evaluate the Performance of a Tubular Electrochemical Flow Reactor with Rotating Anode.

S.A. Martínez-Delgadillo[1,*], *J.Ramírez-Muñoz*[2], *H.R.Mollinedo*[3], *O.M.Huerta*[4], *C.Barrera-Diaz*[5] *and V.X.Mendoza-Escamilla*[6]

[1]Depto. Ciencias Básicas. Universidad Autónoma Metropolitana Azcapotzalco. Av. San Pablo 180. Azcapotzalco. CP 02200, México D.F. México.
[2]Depto. Energia,. Universidad Autónoma Metropolitana Azcapotzalco. Av. San Pablo 180.
[3]UPIITA, Instituto Politécnico Nacional. Av.IPN 2580, Ticoman. México D.F.
Azcapotzalco. CP 02200, México D.F. México.
[4]SEPI. ESIME, Instituto Politécnico Nacional. U. P. Ticomán. México D.F.
[5]Centro Conjunto de Investigación en Química Sustentable UAEM UNAM, Carretera Toluca-Atlacomulco, km 14.5,Unidad El Rosedal, C.P. 50200, Toluca, Estado de México, México.
[6]Depto. Electrónica. Universidad Autónoma Metropolitana –Azcapotzalco. Av. San Pablo 180. Azcapotzalco. CP 02200, México D.F. México.
[*]E-mail: samd@correo.azc.uam.mx.

Received: 24 November 2012 / *Accepted:* 26 January 2013 / *Published:* 1 March 2013

In the present work, Computational Fluid Dynamics (CFD) analysis was used to evaluate the dispersion and visualize the velocity and vorticity field behavior along of a tubular electrochemical reactor in laminar flow regime, with a low speed-rotating anode operated. Five different reactor configurations to evaluate the performance of the reactor with rotating anode (cases C and D) in comparison with the reactor with static electrodes (cases A, B and E) were tested. Configurations A, E and C have three gaskets between the cathode and the anode. In the case E, the anode area was doubled to evaluate the effect on the reactor performance. At the same configuration, with and without gaskets (A versus C and B versus D) a substantial increase in the axial velocity (i.e. a reduction in the backwater), cell Reynolds number and spatial vorticity was achieved operating the reactor with the anode in rotation instead of static one. The improvement with the rotating anode could be related to the reduction of the axial flow barrier and disturbs on the fluid or chaotic flows induced by the motion of the rotating helical electrode. However, the percentage of negative velocities (backmixing) produced with the rotating anode, increased. The reactor with configuration E (static electrode and largest electrode area) showed the highest percentage of low axial velocities. On the other hand, in the flow electrochemical reactor with rotating anode, the backwater (low axial velocities ±0.0002 m/s), were reduced significantly. The vorticity and the cell Reynolds number were evaluated and both increased considerably when the anode was rotated during the electrochemical process, with and without gaskets. However, the percentage of negative velocities produced with the rotating electrode, increased until values higher than 55.25%.

Keywords: CFD simulations, electrochemical, hexavalent chromium, rotating anode, tubular reactor.

1. INTRODUCTION

The electroplating, leather tanning, and textile industries play an important role in production processes and economical Mexican activity. However, these industries commonly are small facilities, which in most cases, cannot afford the commercially available technologies to remove chromium (VI) from wastewaters (i.e. the use of bisulphite, evaporation, ion exchange, and ferrous sulphate, among others), due to some drawbacks such as the high investments and operation costs. Such technologies also generate high quantities of sludge, which need additional treatment, handling, and disposal, raising even more the cost of the processes. As a result, small industries release to the sewage, relatively large amounts of Cr(VI) dissolved in their wastewaters. In addition, solid wastes from chromate-processing facilities have been disposed-off improperly in landfills, becoming sources of contamination for groundwater. The former circumstances demand new technologies to treat such hazardous residues. In this sense, electrochemical treatment can be used as an alternative method to reduce Cr(VI) in wastewaters and the associated solid wastes at a reasonable cost.

Electrode materials such as carbon felt electrodes [1] and polypyrrole-coated aluminium electrodes have been proposed [2]. Studies [3] with low cost material electrode (i. e. carbon steel electrodes) have been carried out, removing 99.97% of Cr(VI). In addition, low amount of no hazardous sludge were generated and it contains chromite ($FeCr_2O_4$) [4], which has refractory properties. Moreover, the treated water can be reused in the production process. In this type of reactor, the electrodes play an essential role during the process and its design is very important. They critically affect the flow inside the electrochemical reactor modifying its performance. Different geometries of electrochemical reactors has been used, but their performance has been evaluated as they were a “black box” and only few studies [5-8] have addressed the impact of the hydrodynamic parameters on the reactor performance. The state-of-the-art CFD tool [5-12], allows us to know a detailed velocity and vorticity distribution map for the fluid inside the reactor during the processes. By CFD tools, it has been demonstrated that the reactor inlet type has an important influence on reactor performance affecting the backmixing degree or dispersion [5]. In other studies, CFD tool has been used to evaluate the reactor behaviour, but using only static electrodes [6]. It is well-known that a steady laminar flow of a Newtonian fluid in a circular tube produces a steady parabolic velocity profile without radial mixing between fluid layers. Inertial effects on the flow are small at this Reynolds number and the mixing intensity in these systems is inherently non-uniform. Several researches have shown that the only route to fast mixing in laminar applications is via chaotic flows or chaotic mixing [13-15]. Chaotic flows are induced by periodic forced changes in the motion direction of the fluid using mixing equipment such as static mixers, in-line dynamic mixers or mechanically stirred tanks. The static mixers are based on the principle of moving the streams radially imposing spatial periodicity. In the case of stirred tank, each passage of the impeller blades – still operating at a constant speed- disturbs the fluid periodically. The in-line dynamic mixers in laminar flow include a variety of rotating screw devices whose principle of operation is similar to the static mixers, but with rotating elements -similar

to the one that is proposed in the paper- that contributes to chaotic mixing, i.e. intensifies the mixing process.

The objective of this work is to evaluate the dispersion and visualize the velocity and vorticity fields along the tubular reactor with a rotating anode, operated in the laminar flow regime. In addition, studies with a reactor with static electrode were carried out and the results were compared with those ones obtained with the reactor with rotating anode. In the study, five different reactor configurations were tested and compared; operating the reactor with the anode in rotation (cases C and D), while the others were with a static anode (cases A, B and E). To obtain an effective motion of the streams radially, like the one produced by a static mixer, three configurations of the electrochemical reactor were simulated with a static long helical electrode, which also serves as a sacrificial anode (cases A, B and E). In the case E, the anode area was doubled to evaluate the effect on the reactor performance. On the other hand, considering that the process efficiency is gradually reduced during the electrochemical process in reactors with static electrodes, due to the passivation effect of the oxide film that builds up on the anode surface [3, 19]; the two remaining configurations were carried out operating the reactor with the anode in rotation (cases C and D). Configurations A, E and C have three gaskets, which acts as insulators between the cathode and the anode. According to our review of the literature on this topic, no previous work has compared the performance of static with rotating anode in electrochemical reactors. The motion of the helical anode was induced with the purpose of producing an additional chaotic mixing inside the reactor and accelerating the mixing process by bringing the components into more intimate contact, i.e. similar to that produced by rotate screw devices in laminar flow. Because the degree of axial mixing affects the conversion and yield in reactors [6, 16, 17], a pulse of an inert tracer injected at the reactor inlet was simulated and its behavior was evaluated monitoring its concentration at the reactor outlet [18]. Based on these simulations, the exit age distribution function (E), the dispersion number (Nd) and the residence time in the reactor were obtained for each reactor configuration.

2. MATERIALS AND METHODS

The electrochemical tubular reactor of carbon steel material, shown in Figure 1, was used during the experimentations. The operation volume was 2.28 L and its dimensions were 1.05 m length and 0.054 m internal diameter (ID), as shown in figure 1. A central polished carbon steel rod measuring 1.05 m served as cathode, giving a 0.0094 m^2 cathode surface area, for all cases. The same material and ID were used to make a 3.0 m (case A, B,C and D) and 5.356 m long helical wire (case E), to serve as anode with areas of 0.05654 and 0.101 m^2, respectively. For case A, E and C, the anode was isolated from the cathode by three rubber gaskets. The flow rate of the electrochemical reactor was regulated to keep the inlet flow velocity at 0.0481 m/s. Simulations with the same flow velocity inlet were carried out in cases C and D, operating the reactor a rotational anode speed of 6.28 rad/s. The configurations tested were as shown in table 1.

Table 1. Electrochemical reactor configurations for each case.

Case	Gaskets	Rotational anode speed (rad/s)
A	3	0
B	no	0
E	3*	0
C	3	6.28
D	no	6.28

*Longer anode.

Fluent version 6.3 has been used to perform the CFD three-dimensional simulations at the steady (fully developed flow) and unsteady state fluid flow (tracer tests).

During the simulation, the laminar model equations have been solved considering the operation in low Reynolds Numbers and the limiting form of the equations of motion, where μ and λ represent the first and second viscosity coefficient, respectively. The full equations (1 to 2) of motion for a three-dimensional flow are:

$$\frac{\partial \rho}{\partial t} + \nabla \cdot \left(\rho \vec{V}\right) = 0 \quad (1)$$

$$\rho\left[\frac{\partial \vec{V}}{\partial t} + \left(\vec{V} \cdot \nabla\right)\vec{V}\right] = -\nabla \bar{p} + \frac{1}{Re}\left(\nabla\left[\lambda\left(\nabla \cdot \vec{V}\right)\right] + \nabla \cdot \left[\mu\left(\nabla \vec{V} + \nabla \vec{V}^{T}\right)\right]\right) \quad (2)$$

A solution of these limiting equations may then reasonably be expected to describe approximately the flow in a laminar boundary layer for which Re is large but not infinite. Where ρ represent the density and $\vec{V}$ the velocity vector in all three directions, $\bar{p}$ is the fluid pressure.

Inside the boundary layer, viscous forces balance inertia and pressure gradient forces. In other words, inertia and viscous forces are of the same order as seen in equation 3.

$$\frac{\bar{\nu}}{\bar{U}_{\infty}\bar{L}}\left(\frac{\bar{L}}{\delta}\right)^{2} = O(1) \ldots\ldots \Rightarrow \ldots\ldots \delta = O\left(Re^{-1/2}\,\bar{L}\right) \quad (3)$$

Therefore, the boundary layer thickness δ is a function of $\bar{L}$ and the square root of Re at $x = \bar{L}$ position.

The variables, denoted with an over bar, must be dimensionless (letters without over bar) using the reference length ($\bar{L}$) and the free-stream velocity ($\bar{U}_{\infty}$). Then, the dimensionless variables related to their corresponding dimensional counterparts are shown in equations 4 and 5.

$$x = \frac{\bar{x}}{\bar{L}}, y = \frac{\bar{y}}{\bar{L}}, z = \frac{\bar{z}}{\bar{L}}, t = \bar{t}\frac{\bar{U}_{\infty}}{\bar{L}} \quad (4)$$

$$u = \frac{\bar{u}}{\bar{U}_{\infty}}, v = \frac{\bar{v}}{\bar{U}_{\infty}} Re^{1/2}\, w = \frac{\bar{w}}{\bar{U}_{\infty}}, p = \frac{\bar{p}}{\bar{P}_{\infty}} \quad (5)$$

With the Reynolds number defined as $\mathrm{Re} = \frac{\overline{U}_\infty \overline{L}}{\overline{\nu}}$, where $\overline{\nu}$ is the kinematic viscosity. The non-dimensional vorticity components are given by the rotational (equation 6).

$$\omega_x = \frac{1}{\mathrm{Re}}\frac{\partial v}{\partial z} - \frac{\partial w}{\partial y}, \omega_y = \frac{\partial w}{\partial x} - \frac{\partial u}{\partial z}, \omega_z = \frac{\partial u}{\partial z} - \frac{1}{\mathrm{Re}}\frac{\partial v}{\partial x} \tag{6}$$

As mentioned above, during the simulations, the Navier-Stokes equations are used in a conservative formulation for laminar flow (in an inertial non-accelerating reference frame), see equation 7.

$$\frac{\partial(\rho\vec{V})}{\partial t} + \nabla\cdot(\rho\vec{V}\vec{V}) + \nabla p = \nabla\cdot(\bar{\tau}) \tag{7}$$

And continuity in equation 8.

$$\nabla\cdot\vec{V} = 0 \tag{8}$$

where $\bar{\tau}$ is the stress tensor given by equation 9,

$$\bar{\tau} = \mu\left[\left(\nabla\vec{V} + \nabla\vec{V}^T\right) - \frac{2}{3}\nabla\cdot\vec{V}I\right] \tag{9}$$

where I is the unit tensor, and the second term on the right hand side is the effect of volume dilation.

A pressure-based segregated algorithm solver has been used, where the governing equations are solved sequentially. For the pressure-velocity coupling a non-linear algorithm called Semi-implicit pressure-linked equation (SIMPLE) was used, for pressure discretization the Standard scheme was selected, and for the momentum discretization, the Second Order Upwind scheme was applied. To simulate the tracer injection, a tracer pulse with the same material properties of the working fluid and a concentration of unity, was applied for one second at the inlet surface. Then, the conservation equations were solved. Fluent calculates the local mass fraction of each species and then the concentration of the tracer was monitored at the outlet surface to obtain the age distribution function (**E**) and the dispersion number (Nd) was evaluated. The model was validated experimentally in a previous work [6, 19]. It was considered that the electrochemical reactor was a closed vessel. The equation (10) was used to evaluate the mean residence time and equation (11) to evaluate the Nd. This method is reliable to use when Nd <1 [18].

$$\mathrm{th} = \frac{\int_0^\infty tCdt}{\int_0^\infty Cdt} \tag{10}$$

$$\frac{\sigma^2}{th} = 2\left(\frac{D}{uL}\right) - 2\left(\frac{D}{uL}\right)^2\left(1 - e^{(uL/D)}\right) \quad (11)$$

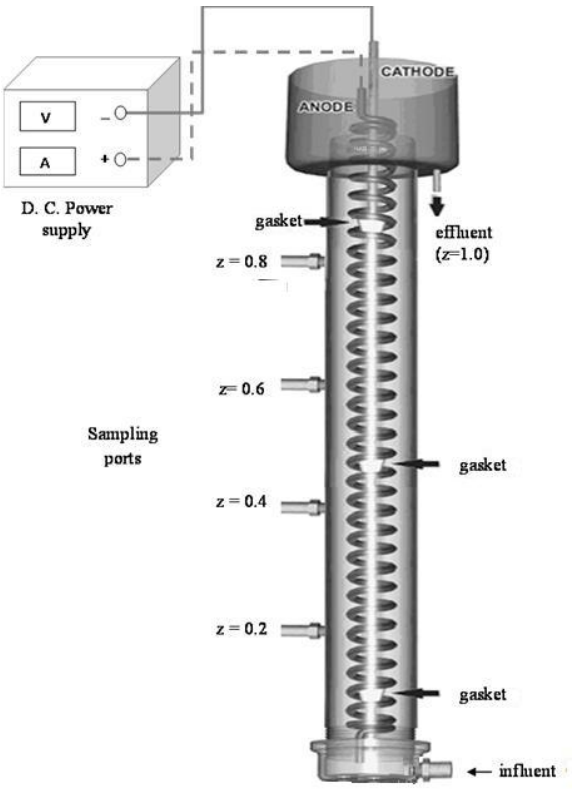

Figure 1. The schematic diagram of the electrochemical tubular reactor

Where: t = time (min); C= tracer concentration (mg/L); σ^2 = variance (min^2), th = mean residence time (min), *D* = dispersion coefficient ($m^2\ s^{-1}$), *u* = flow velocity (m/s), $\bar{L}$ = reactor length (m), **E =** exit age distribution function (min^{-1}), $\theta = t/th$ (dimensionless) and $Nd = \frac{D}{u\bar{L}}$.

3. RESULTS AND DISCUSION

The axial velocity profiles along the reactor for the reactor with the static anode are shown in figure 2; with three gaskets (case A), without gaskets (case B) and with three gaskets and longer anode (case E). As seen, case E exhibits more uniform axial velocities along the reactor than in case A and B, but as the flow approaches to the reactor outlet, the axial velocity increases considerably. In the cases A and E, there are no negatives axial velocities along the reactor above 0.2 m of the reactor length, and the higher axial velocities were reached near the reactor outlet. The percentage of low axial velocities (±0.0002m/s) in the case E is 20.9%, while in the cases A and B are 16.74% and 15.67%, respectively, which means that case E exhibits the highest backwater of all the configurations.

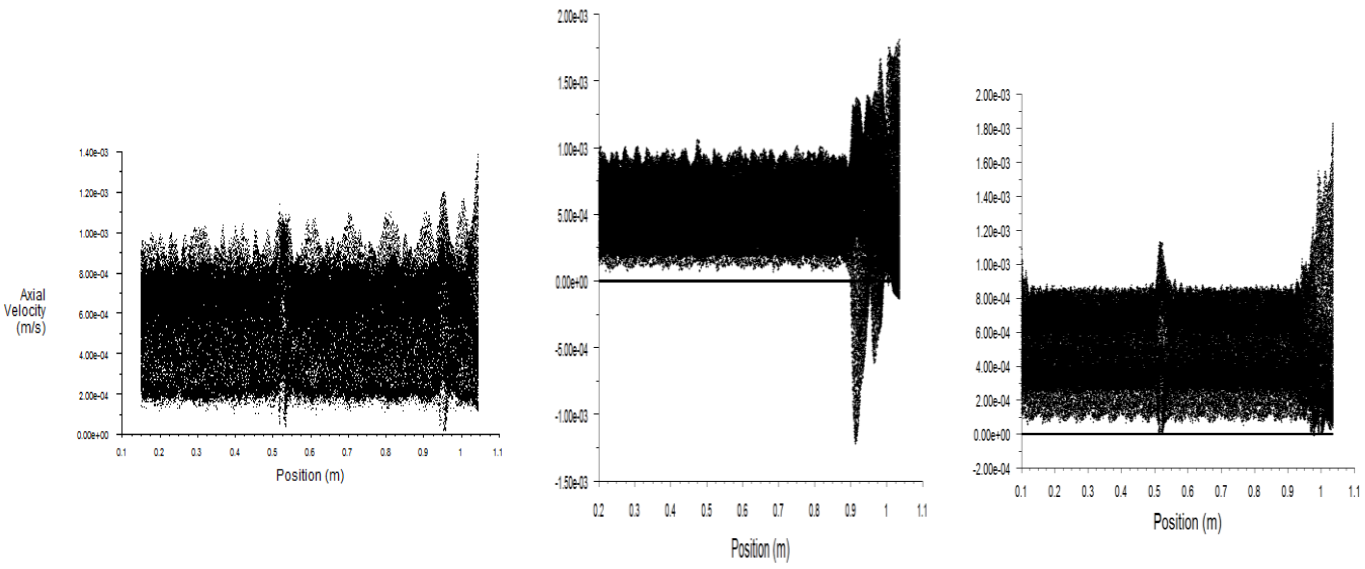

case A case B case E

Figure 2. Axial velocity profiles along the reactor with the static anode.

A greater number of turn helical wires in the case E increase the solid surface in contact with the downstream velocity profile, which also increases the total fluid drag on surface.

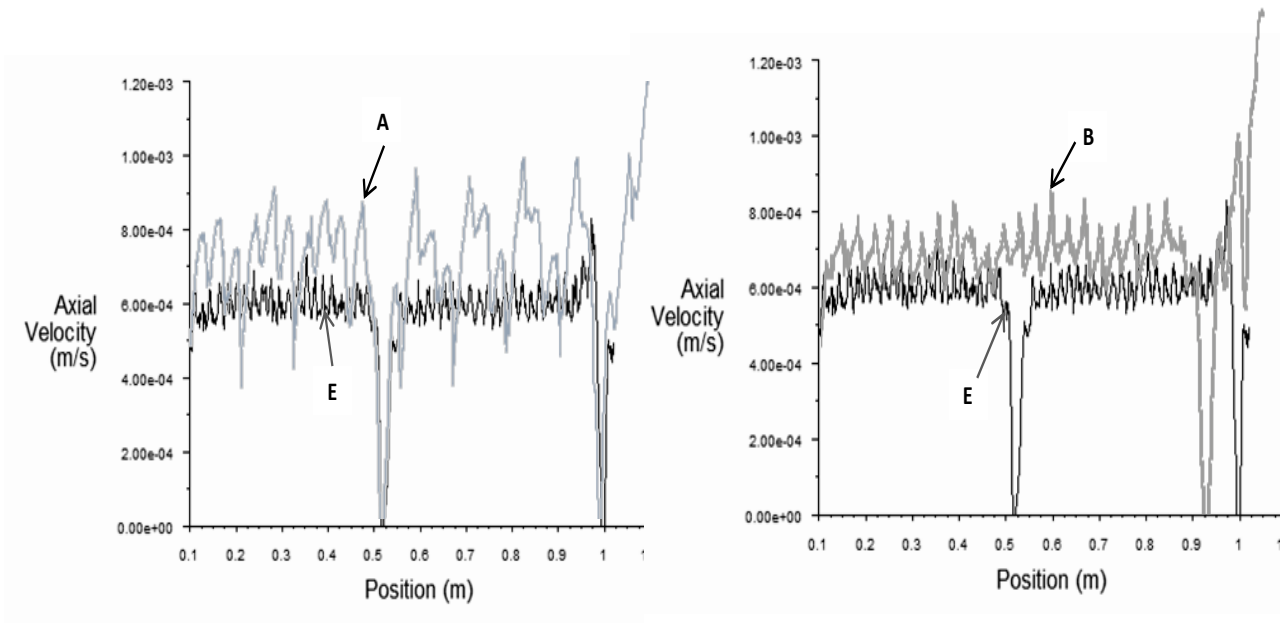

(a) (b)

Figure 3. Comparison of the axial velocity along the reactor in case E with: a) case A and (b) case B.

According to these results, the magnitude of the depression in the velocity profile for this case can be directly associated with the increasing skin drag on the solid electrode surface. Figure 3 compares the axial velocities of case E along the reactor, with respect to axial velocities of cases A and B. The velocities were evaluated along the reactor between the cathode and the anode. For case E, lower axial velocities than those obtained for cases A and B are reached, as shown in figure 3(a) and 3(b), respectively. Figure 4, shows the pathlines (in grey scale) that individual fluid particles follow along the reactor for case E and A. It should be noted that, in the case E, the pathlines are more rectilinear than in case A and B (not shown), i.e. the intermixing between fluid layers is lower in case E. As a result, there is lower mixing in case E than in case A and B. This effect could cause less contact among species in the fluid and with those released from the electrodes. Additionally, it means less contact of dissolved species in the fluid with the electrodes surface, and consequently, case E can be expected to have a lower efficiency.

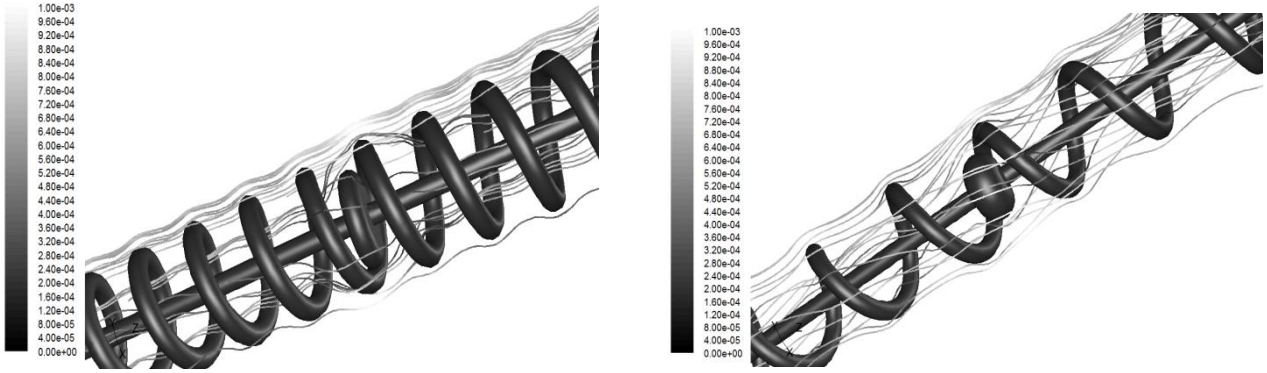

case E case A

Figure 4. Pathlines in grey scale by axial velocity for case E and A.

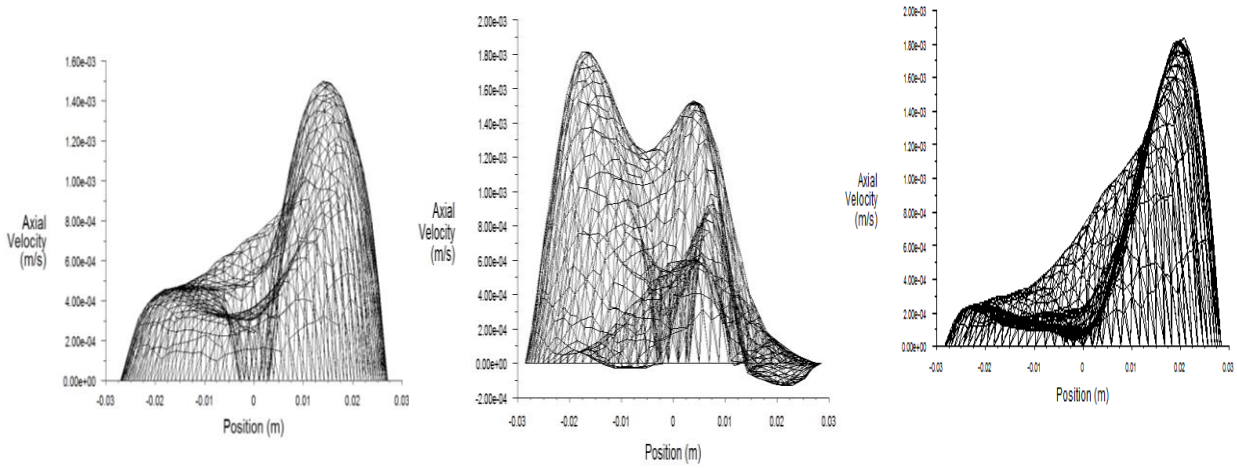

case A case B case E

Figure 5. Axial velocity profiles at the surface outlets of the different reactor configurations.

Figure 2 shows for case B, that there are high axial velocities positives and negatives near the outlet. Figure 5 illustrates the axial velocity profiles at the surface outlets for A, B and E configurations are shown. As can be seen, only in case B there are negative axial velocities near the reactor exit. The percentage of elements at the outlet surface with negative axial velocities is 10.025%, while in case A and E is 0%. On the other hand, the percentage of negative axial velocities in the reactor with configuration A and E are 3.05%, and 3.16%, respectively, while in case B the percentage reaches 5.37%.

As shown in figure 2, the axial velocity profile in cases A and E exhibit fewer variations at the reactor outlet than in case B. The negative flow in case B, produced a longer tail than in case A and E, due to the long-lived material leaving the reactor, as shown in the exit age distribution curve for fluid flowing through the electrochemical reactor (Figure 6). This effect increased the dispersion number in case B (Nd=0.052) compared to case A (Nd=0.041) and E (Nd=0.043). In addition, the higher percentage of low axial velocities (±0.0002m/s) in the case E, also implies, the lowest average axial velocity ($5.349x10^{-4}$ m/s) and the longest residence time (29.67 min). In case B, the average axial velocity was $5.514\ x10^{-4}$ m/s and the residence time 28.7 min, for case A these parameters were $5.733\ x10^{-4}$ m/s and 27.68 min, respectively. As seen, although the case E exhibits the highest backwater, the results show that, with the static electrode, the negative axial velocity at the electrochemical reactor outlet has an important effect on the reactor dispersion.

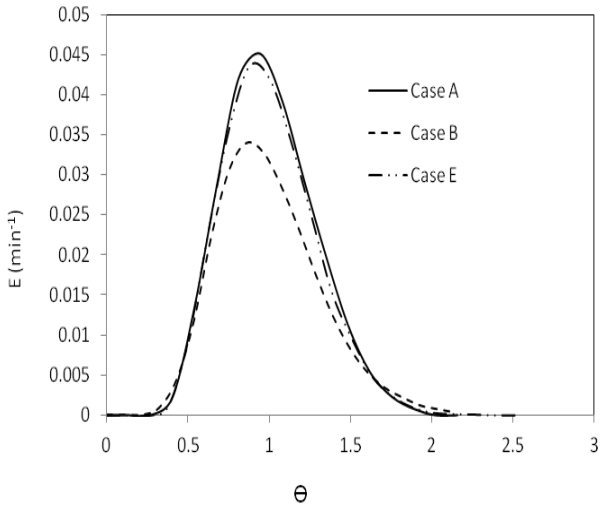

Figure 6. The exit age distribution curve E for fluid flowing through the electrochemical reactor for cases A, B and E.

Simulations with configurations similar to those of cases A and B were performed, so as to improve the contact among species in the fluid and to increase the relative velocity between the electrodes surface and the liquid. The intention was to perturb the flow and mix the streams that contained Cr (VI) and Fe (II) ions. Such cases are C and D. For these configurations, the electrodes were rotated at angular velocity of 6.28 rad/s, as indicated in table 1. The low angular velocity of

anode was used to improve the mixing, reduce the backwater, maintain low dispersion in the reactor and then enhance the electrochemical reactor performance. Figure 7 shows the axial velocity profiles inside the electrochemical tubular reactor for cases C and D. It can be seen that the axial velocities increased in about one order of magnitude due to the electrode rotation, and the backwater was reduced in both cases because the percentage of low axial velocity components was reduced by 3.42% in case C and 3.05% in case D. In both cases, the cell Reynolds number average increase from 1.2, case A, to 26.2, case C, and from 1.13, case B, to 25.07, case D.

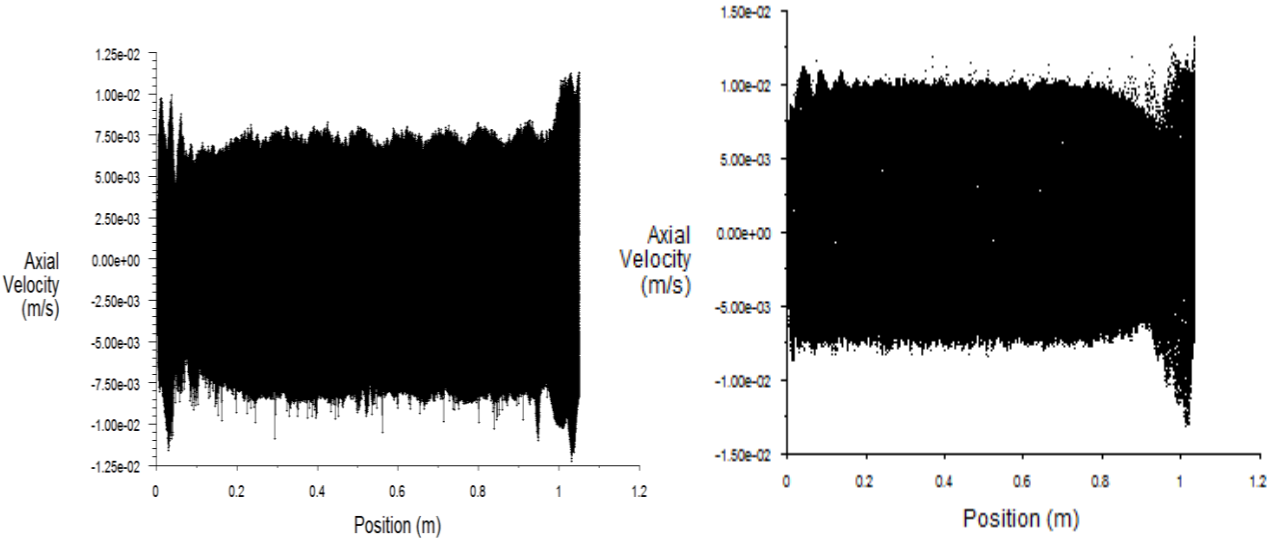

Case C Case D

Figure 7. Axial velocity profiles for case C and D, in the electrochemical tubular reactor.

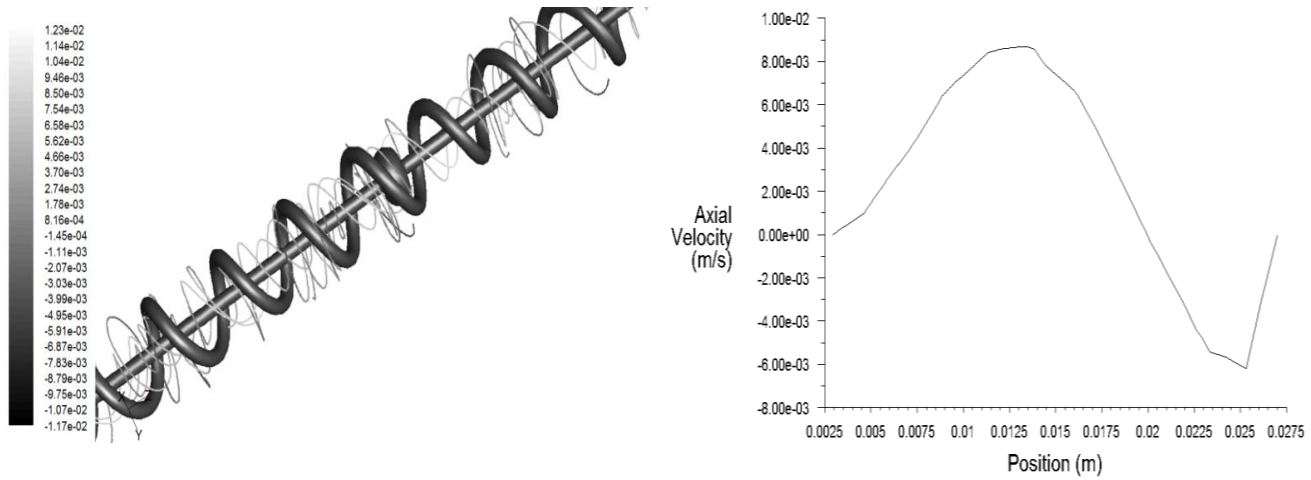

(a) (b)

Figure 8. Case C: (a) Pathlines in grey scale by axial velocity and (b) axial velocities at radial position

The magnitude of the vorticity in both cases, C (5.141s^{-1}) and D (5.26 s^{-1}) is much higher than in cases A (0.173 s^{-1}), B (0.184 s^{-1}) and E (0.185s^{-1}). This is due to the rotational motion of the electrode that also produces a higher percentage of negative axial velocities, 55.27% in case C and 53.2% in case D, more than 50%, than in case A and B, as shown before. Faster reactions (e.g. Cr(VI) reduction into the solution by using ferrous ions Fe(II)) and solid–liquid mass transfer (e.g. the releasing ferrous ions (Fe (II)) from the anode into the solution) will be favored increasing both, the local mixing rates and the velocity gradients at the solid-liquid interface. On the other hand, it is widely recognized in stirred tanks that maximum vorticity values and higher local mixing rates are obtained in regions near the impeller where steep normal gradients occur in the velocity. Therefore, it should be expected that increasing the vorticity by rotating the electrodes enhances local mixing and increased the anode–liquid mass transfer, i.e. promotes that the two reactants Cr (VI) and Fe (II) are brought together and causes a higher mass transfer between the electrodes and the liquid. Figure 8(a), shows the pathlines in grey scale by axial velocity for case C (rotating electrode). As seen, fluid particles move around the electrode following a helical trajectory and improving the intermixing between the layers of fluid, i.e. improving the contact between the species in the fluid and with the electrode surface. Moreover, figure 8(b), shows that the velocity changes from positive, between the central electrode (cathode) and the helical anode, to negative values, between the helical anode and the reactor wall, generating a better mixing along the reactor. Figure 9, shows the sweep surface velocity axial vectors for both cases: static and rotating helical electrode.

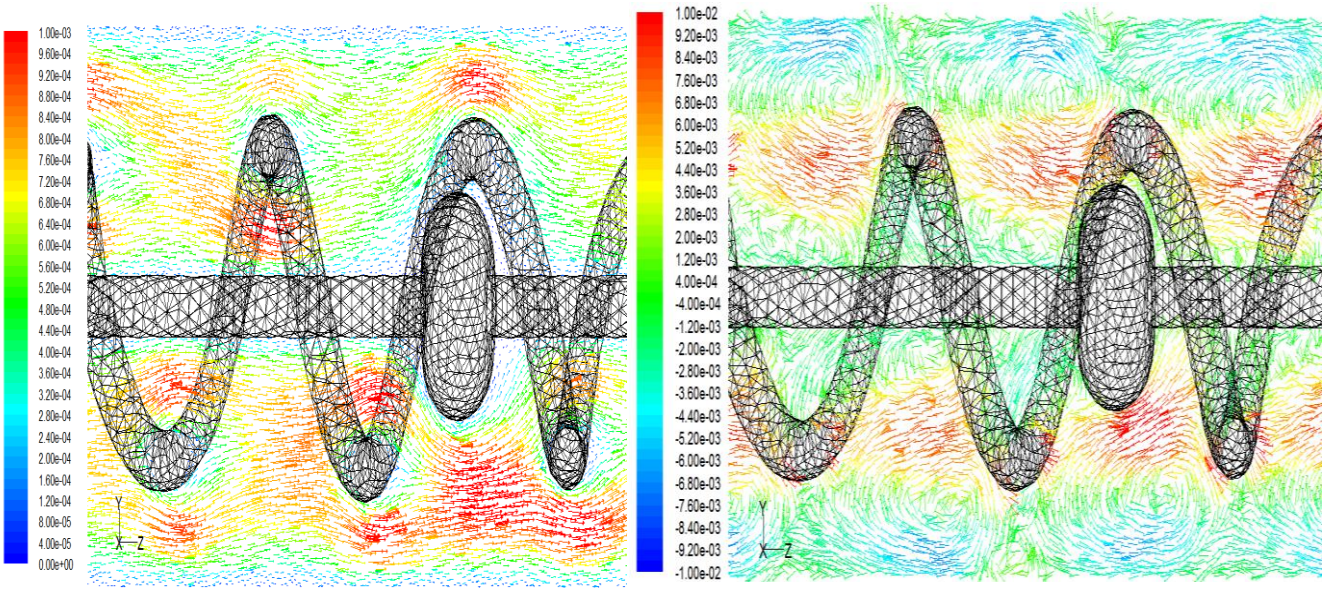

Static helical electrode Rotating helical electrode

Figure 9. Velocity axial vectors for static and rotating electrodes.

Because the velocities with static electrodes are lower than with the rotating ones, the scales in both figures are different to emphasize the effect of the rotating electrode in the velocity. As see, in the

first case (static electrode), the axial velocity is lower than in the case of the rotating electrodes and the velocity axial vectors show that there is a low relative velocity between the reactor wall and the electrodes with respect to the liquid, i.e. lower local shear rate or agitation intensity. In contrast, for the rotating electrode, the axial velocity is higher and the streams move from the wall reactor to the electrodes in a circular way. In this manner, the thickness of the boundary layer is minimized improving mass transfer between the electrodes and promoting the contact among species in the fluid. Thus, the reactor performance is improved.

Other authors have carried out studies with a similar tubular electrochemical reactor with static mesh electrodes to improve the reactor performance [7]. However, in that reactor, there are zones between the reactor wall and the mesh electrodes where velocity reaches twice the velocity found in between the electrodes. Therefore, in those zones, there is more short-lived material leaving the reactor reducing its performance. In addition, due to the low mixing, the reaction zone is restricted to the zone between the electrodes mesh and the effective reaction volume in the reactor is reduced. On the other hand, in the reactor with rotating helical electrode, there are no zones with low mixing (figure 9); the short-lived reactants are reduced and the effective reactor volume is higher than in the reactor with the reactor mesh electrodes.

When the electrochemical reactors were simulated with rotating electrodes, negative axial velocities or backmixing are produced at the reactors outlet, as shown in figure 10. In case C, 49.76% of the elements at the outlet surface exhibit negative axial velocity while in case D, a higher percentage (51.29%), showed negative axial velocity.

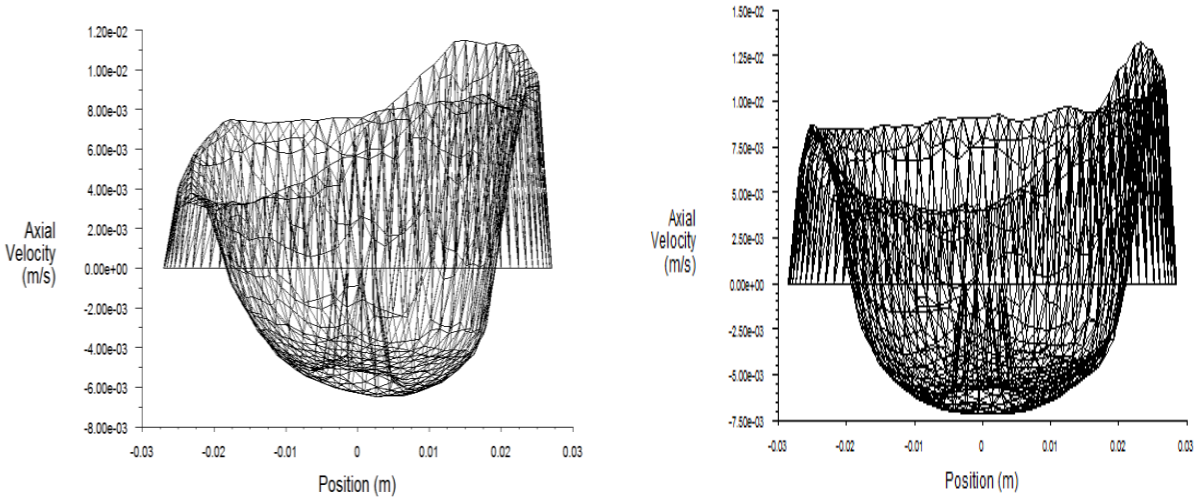

case C case D

Figure 10. Axial velocity profiles at the surface outlets of the C and D reactor configurations

The rotational motion of the helical electrode increased the dispersion in the reactors; in the case C the Nd was 0.076, while in case D the Nd increased at 0.085. The higher dispersion observed for case D can be explained because there is more long-lived material leaving the reactor than for case

C. As already mentioned, for case D, there are more negative axial velocities at the reactor outlet than for case C and such behaviour produces a longer tail in exit age distribution curve for case D, as shown in figure 11(a).

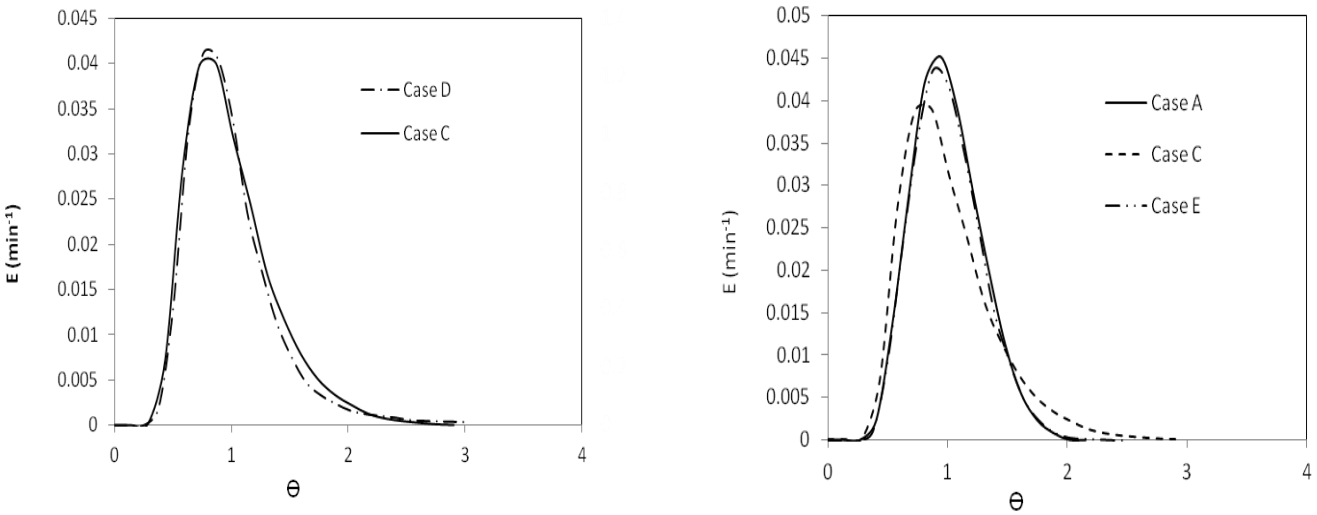

(a) (b)

Figure 11. The exit age distribution curve **E** for fluid flowing through the electrochemical reactor for: (a) cases C and D and (b) cases A, C, and E.

These phenomena caused that in case D, the average axial velocity in the fluid (5.46 x10^{-4} m/s) was lower than in case C (5.647 x10^{-4} m/s). Figure 11b, shows the exit age distribution curve (E) for the three cases with gaskets, A, E and C. As shown, there is more short-lived material leaving the reactor in case C than in case A and E, due to the higher percentage of axial negative velocities or backmixing, which increased the contact time between the two reactants Cr (VI) and Fe (II) and the dispersion in the reactor. Although the reactor operated in configuration A provided the lowest dispersion, it is also important to have good mixing in the reactor, to allow the contact between the species in the fluid and the mass transfer between the electrodes and the fluid. Therefore, the higher mass transfer between the electrodes and the liquid will increase the electrochemical reactor performance. Consequently, the mixing effect must not be so high, because an increasing dispersion in the reactor reduces its efficiency.

4. CONCLUSIONS

The effects of different configurations for an electrochemical flow reactor with a static anode and with an anode in rotation were investigated in this work. It was found that the type of electrochemical reactor configuration affects its performance. The reactor operated with static anode

and with gaskets presented the lowest dispersion among the configurations tested. The rotating electrode causes that the axial velocity, the vorticity diffusion and the Cell Reynolds Number Average (i.e. the flow regime) increase in the reactor. These effects increase mass transfer between the electrodes and the liquid, and a better intermixing between layers of fluid. Moreover, the backwater is reduced when the electrode is rotated. The negative axial velocity at the electrochemical reactor outlet has an important effect on the reactor dispersion. By using CFD tools, it was possible to obtain the axial velocity profiles within the reactor for different operational conditions and to find out and estimate the fluid behavior within the electrochemical reactor.

ACKNOWLEDGEMENTS
Financial supports of this work by the Consejo Nacional de Ciencia y Tecnología (Proyecto:CB-2011/169786) are gratefully acknowledged.

References

1. I. Frenzel, H. Holdik, V. Barmashenko, F.D. Stamatialis, M. Wessling, *J. Appl. Electrochem*. 36 (2006) 323
2. K. G.Conroy and C. B. Breslin, *J Appl Electrochem* 34 (2004) 191
3. S.A. Martinez, and M. G. Rodriguez, *J. Chem. Technol. Biotechnol*, 82 (2007) 582
4. N. Kongsrichroern, C. Polprasert, *Water Sci. Technol.* 31 (1995) 109
5. S. A. Martinez-Delgadillo, H. R. Mollinedo-Ponce , M. Gutiérrez-Villegas, I. B. Q. and J. M. M., *Comput. Chem. Eng.* 34 (2010) 491
6. S. Martinez-Delgadillo, H. Mollinedo-Ponce, V. Mendoza-Escamilla, and C. Barrera-Díaz, *Chem. Eng. J.* 165 (2010) 776
7. J. Su, H.Y. Lu, H. Xu, J.R. Sun, J.L. Han and H.B. Lin, Russian Journal of Electrochemistry. 47 (2011) 1293
8. A.Frías-Ferrer, I.Tudela, O. Louisnard, V. Sáez, M. Esclapez, M. Díez-García, P.Bonete and J. González-García, *Chem. Eng. J.* 169 (2011) 270.
9. A. V. Atilano, H. F. Meier, J. J. Iess and M. Mori, *Ind. Eng. Chem. Res.*, 47 (2008) 192
10. J. M. Zalc, E. S. Szalai, M. M., Alvarez and F. J. Muzzio, *AIChE J.*, 48 (2002) 2124
11. A. A. Kulkarni and V. V. Ranade, *AIChE J.*, 54 (2008) 1139
12. J.L.C. Santos, V. Geraldes, S. Velizarov, J.G. Crespo, *Chem. Eng. J.* 157 (2010) 379
13. T. Avalosse and M. J. Crochet, AIChE J., 43(1997). (3), 588–597
14. D. M., Hobbs, M. M. Alvarez and F. J. Muzzio, *Fractals*, 5 (1997) 395
15. D. R. Unger, and F. J. Muzzio, *Can. J. Chem. Eng.*, 76 (1998) 546
16. K. Ekambara and J. B Joshi, *Chem. Eng. Sci.*, 59 (2004) 3929
17. S. D. Sandesh, M. J. Sathe and J. B. Joshi, *Ind. Eng. Chem. Res*, 48 (2009) 37
18. O. Levenspiel, *Chemical Reaction Engineering*; John Wiley & Sons, New York (1999).
19. S. Martinez-Delgadillo, V. Mendoza, H. Mollinedo-Ponce, H. Puebla, J. M. Méndez-Contreras, *Ind. Eng. Chem. Res*. 5 (2010) 2501